

ARTICLES

Wall migration and shear-induced diffusion of fluid droplets in emulsions

S. D. Hudson

Polymers Division, National Institute of Standards and Technology, Gaithersburg, Maryland 20899-8544

(Received 8 August 2002; accepted 21 January 2003; published 21 March 2003)

The spatial distribution of drops in multiphase Stokes flow is derived theoretically as a function of two dimensionless parameters, accounting for wall migration, buoyancy, and shear-induced diffusion. The wall migration effect, which drives drops away from the walls and toward the center of the gap, is often significant even when droplets are 100 times smaller than the gap. By comparison with the experimental drop concentration profile, the shear-induced down-gradient diffusivity is measured and found to be approximately four to five times larger than the prediction for drop *self-diffusivity*. These are the first such measurements of the diffusivity of drops with clean interfaces and contrast markedly with previous measurements on surfactant-laden drops. Nonuniform concentration along the vorticity axis is also investigated briefly.

[DOI: 10.1063/1.1560617]

I. INTRODUCTION

Immiscible fluid mixtures are encountered in many industrial processes, and the distribution and shape of the disperse phase in such fluids is of interest. In addition to bulk phenomena, wall effects may become significant when small distances separate the bounding walls, see, e.g., Ref. 1. Greater understanding of multiphase flow in narrow passages may aid development of microfluidic applications, particularly those concerning liquid–liquid separation.

In bounded uniform shear flow, fluid droplets are known to migrate away from the walls and toward the center plane of the shear cell (see, e.g., Ref. 2). Small deformation theory^{3–7} predicts the migration velocity $u_{\text{mig, single}}$ away from a single wall:

$$u_{\text{mig, single}} = \alpha \text{Ca} \dot{\gamma} a \frac{a^2}{y_1^2}, \quad (1)$$

where y_1 is the distance from the wall to the center of the drop, a is the droplet radius, and $\dot{\gamma}$ is the shear rate. α is a coefficient (equal to approximately 0.6, with slightly different values for each of the predictions cited) that is a very weak function of the ratio $\hat{\eta} = \eta_d / \eta_c$ between droplet and continuous phase viscosities [see Eq. (3)]. Ca is the capillary number equal to $\eta_c \dot{\gamma} a / \sigma$, where σ is the interfacial tension.

Experimental measurements^{2,6,8,9} and simulations^{10–12} of $u_{\text{mig, single}}$ are within several percent of the predictions of small deformation theory [Eq. (1)] when $\hat{\eta} < 1$, but poor agreement is observed when $\hat{\eta}$ is large. Even when $\hat{\eta} < 1$, significant deviations (nearly 40%) between simulation and small deformation theory are observed when y_1/a is small, i.e., equal to 2.5.¹¹ Moreover, these simulations show that α also depends weakly on Ca when y_1/a is small,^{10,11} suggest-

ing that the assumptions of small deformation theory do not hold when the drops are within a few radii from the wall.

The prediction of Chan and Leal accounts for the effect of both walls simultaneously:⁵

$$u_{\text{mig}} = 4\alpha \text{Ca} \dot{\gamma} a \frac{a^2}{h^2} \left(-y' - \frac{8y'}{(1-4y'^2)^2} \right), \quad (2)$$

where y' is the dimensionless position from the center plane between bounding walls separated by a distance h . The second term in Eq. (2) is always the most significant and is equivalent to the simple sum of the effect of each wall individually. According to Chan and Leal, the coefficient α is written

$$\alpha = \frac{(16 + 19\hat{\eta})}{(16 + 16\hat{\eta})} \frac{3(54 + 97\hat{\eta} + 54\hat{\eta}^2)}{280(1 + \hat{\eta})^2}. \quad (3)$$

Drops also drift in response to buoyant force:¹³

$$u_{\text{buoy}} = -\frac{2}{9} \frac{(\rho_d - \rho_c)g}{\eta_c} \frac{(\hat{\eta} + 1)}{(\hat{\eta} + 2/3)} a^2, \quad (4)$$

where ρ_d and ρ_c denote the density of the respective phases. The ratio

$$\beta = \frac{1}{18\alpha} \frac{\text{Bo}}{\text{Ca}^2} \frac{h^2}{a^2} \frac{(\hat{\eta} + 1)}{(\hat{\eta} + 2/3)},$$

which depends strongly on Ca , assesses the relative importance of buoyancy and wall migration. $\text{Bo} = -(\rho_d - \rho_c)ga^2/\sigma$ is the Bond number.

When an immiscible mixture contains a sufficient fraction of the droplet phase, then drop interactions are also important. When two droplets on different streamlines collide, their contact is asymmetric and the drops depart on stream-

lines that are more widely separated than the original ones on which they approached one another.¹⁴⁻¹⁷ Random collisions therefore lead to random motions perpendicular to the streamlines.^{15,17} At high rates of flow, droplet motions are dominated by the flow and not by Brownian motion (high Peclet numbers, $Pe_B = 4a^2\dot{\gamma}/D_B$, where the subscript B refers to Brownian diffusion of the drops, thereby distinguishing this Peclet number from the one to be introduced in Sec. II), so that the apparent diffusive motion is called shear-induced diffusion. The self-diffusivity for a monodisperse dilute distribution of droplets is equal to the product of the collision frequency (proportional to $\phi\dot{\gamma}$, where ϕ is the local volume fraction of droplets) and the average square displacement per collision (proportional to a^2):

$$D_{\text{self}} = \phi\dot{\gamma}a^2f_i, \tag{5}$$

where f_i is a coefficient that depends weakly on Ca. The diffusivity is anisotropic, so that the coefficient f_y for diffusion along the velocity gradient is 2 to more than 20 times greater than that along the vorticity axis f_z .¹⁵ f_y and f_z also depend on viscosity ratio $\hat{\eta}$: they are essentially constant for $\hat{\eta} < 0.5$ and approach zero at large relative droplet viscosity.

The diffusion coefficient D describing flux in a concentration gradient is proportional to the self-diffusivity [cf. Eq. (5)]:

$$D = \phi\dot{\gamma}a^2f_{gi}. \tag{6}$$

It turns out that f_{gi} is greater than f_i ,^{15,18} because droplet collisions from the direction of high concentration are more frequent than those from the lower concentration side. As a consequence, f_{gy} is at least twice f_y .¹⁵ For rough hard spheres, $f_{gy} = 6f_y$.¹⁸ For droplets, however, the precise relationship between the two diffusivities has not been established. Here we report the first experimental measurements of the drop diffusivity in emulsions without surfactant.

Shear-induced diffusion and wall migration work against one another, and a nonuniform distribution of droplets is expected at steady state. King and Leighton recently calculated this distribution, assuming a linearized form of the migration velocity.⁹ In this report, we calculate the steady-state distribution of droplets for the unlinearized velocity [Eq. (2)] and compare with experimental results. We also consider the effect of buoyancy. In the nonlinear problem, steady-state solutions are no longer self-similar. Moreover, temporal solutions may be qualitatively different, giving rise to a concentrated layer adjacent to a denuded one near the wall.

II. MODEL CALCULATIONS AND DISCUSSION

First, we assume that the drop size distribution is monodisperse, as is appropriate for steady state.¹⁹ Following King and Leighton,⁹ the local flux of dispersed phase along the velocity gradient direction (y axis) is

$$J = (u_{\text{mig}} + u_{\text{buoy}})\phi - D d\phi/dy, \tag{7}$$

and the corresponding volume fraction balance is

$$\frac{\partial\phi}{\partial t} = -\frac{\partial}{\partial y}[(u_{\text{mig}} + u_{\text{buoy}})\phi - D d\phi/dy], \tag{8}$$

where u_{mig} , ϕ , and D are functions of y . Migration and diffusion along the vorticity axis is ignored.

Substituting Eqs. (2), (4), and (6) into Eq. (8), and non-dimensionalizing, $t = t'(h^2/\dot{\gamma}a^2f_{gy}\phi_0) = t'\tau$, $\phi = \phi'\phi_0$ (where ϕ_0 is the average volume fraction) and $y = y'h$, the governing differential equation is written

$$\begin{aligned} \frac{\partial\phi'}{\partial t'} = \frac{\partial}{\partial y'} \left(\phi' \text{Pe} \left(-\beta + y' + \frac{8y'}{(1-4y'^2)^2} \right) \right) \\ + \frac{\partial}{\partial y'} \left(\phi' \frac{\partial\phi'}{\partial y'} \right), \end{aligned} \tag{9}$$

where

$$\text{Pe} = \text{Ca} \frac{a}{h} \frac{4\alpha}{f_{gy}\phi_0}$$

is a Peclet number, describing the balance of convective (wall migration) to diffusive transport on length scales of the drop radius.

At steady state the net flux is zero, and diffusive and convective fluxes balance. Two solutions of Eq. (9) are possible. One is the trivial solution, i.e., $\phi'(y') = 0$, describing a region free of drops near the wall, demarcated by positions y'_{e-} and y'_{e+} . The other solution is found by integration:

$$\phi'(y') = \phi'_c + \text{Pe} \left(1 + \beta y' - \frac{y'^2}{2} - \frac{1}{1-4y'^2} \right), \tag{10}$$

where ϕ'_c is an integration constant, equivalent to the normalized droplet concentration at the center plane. ϕ'_c is determined by conservation of the total volume fraction, expressed as the following boundary condition:

$$\int_{y'_{e-}}^{y'_{e+}} \phi' dy' = 1. \tag{11}$$

Similar expressions can be derived for pressure driven flow.

Whereas solutions of the linearized problem are self-similar,⁹ nonlinear terms are significant when Pe is small, and the solutions are no longer self-similar (Fig. 1). ϕ'_c and $y'_{e\pm}$ were determined numerically [Eq. (11)] (see Fig. 2), by integrating using the trapezoidal rule and an interval of $\Delta y' = 0.001$. These figures illustrate that the linear solution is a good approximation when Pe is more than 10. When Pe is small, ϕ'_c and $y'_{e\pm}$ approach 1 and ± 0.5 , respectively.

Although the solutions are not self-similar, the effect of average concentration ϕ_0 remains simple. Multiplying Eq. (10) by ϕ_0 , we note that only the first term depends on ϕ_0 (through ϕ'_c as well), so that changing the average concentration simply displaces curves vertically.

Under what circumstances is wall migration significant? Since wall migration is rapid near the wall [Eq. (2)], migration is always significant there, producing a denuded zone, which may be narrow for very small Pe. At larger Pe, wall migration perturbs the drop concentration throughout the bulk. The significance of this bulk effect can be evaluated from the magnitude of either the midplane concentration ϕ'_c or the root-mean-square deviation from the average concentration, $\langle (\phi' - 1)^2 \rangle^{1/2}$. Based on these measures, wall migration has a substantial bulk effect even for small values of Pe,

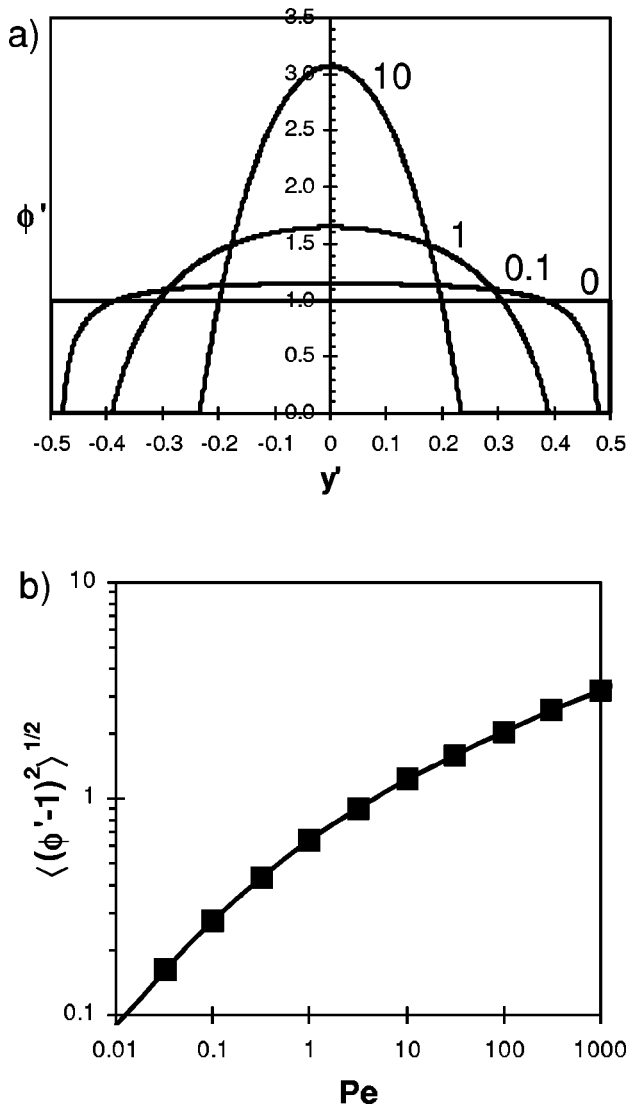


FIG. 1. (a) Normalized steady-state local volume fraction vs dimensionless position within the gap for $Pe=0, 0.1, 1$, and 10 , and $\beta=0$. The concentration profile narrows progressively as Pe increases. (b) The root-mean-square deviation from uniform drop concentration vs Pe .

of order 1 or less. For example, the average deviation of the concentration is 27% when $Pe=0.1$ [Fig. 1(b)]. Considering an emulsion at steady state, for which $Ca \approx 0.4$, $\alpha \approx 0.6$, $f_{gy} \approx 0.2$, $\phi_0 \approx 0.1$, it is remarkable that significant bulk effects occur even when the drop radius is two orders of magnitude smaller than the gap spacing (i.e., when $a/h=0.01$, $Pe \approx 0.5$).

When Pe is changed, the concentration profile evolves toward a new steady state. In the linear model, these temporal solutions are identical in form to the steady-state solutions.⁹ For the nonlinear model, however, temporal solutions are distinct in form. In fact, when Pe is increased, a multimodal distribution may occur in which a peak in concentration forms adjacent to the denuded zone (Fig. 3). The time required to establish the new denuded zone at y'_e is approximated by the following:

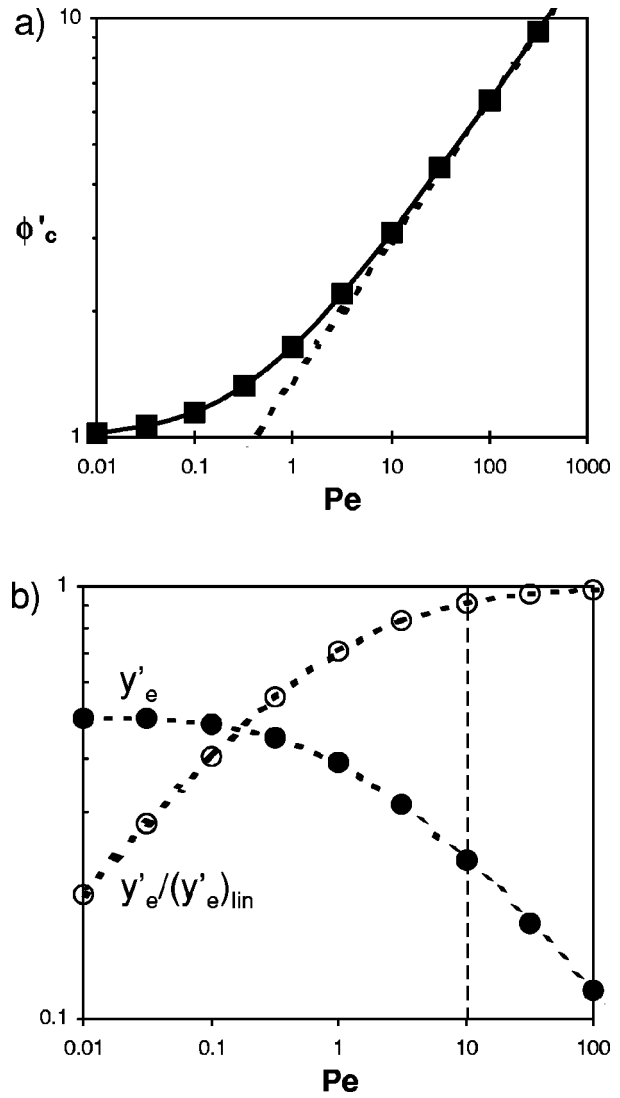


FIG. 2. (a) The integration constant ϕ'_c as function of Pe , and $\beta=0$. The linear solution is shown with dashed line. (b) The edge of the denuded zone y'_e vs Pe (closed symbols), and $\beta=0$. The ratio of y'_e to its linear approximation is plotted with open symbols. When $Pe < 10$, y'_e differs significantly from the linear prediction.

$$\tau_{e\pm}(y'_{e\pm}) = \frac{|\pm \frac{1}{2} - y'_{e\pm}| \cdot h}{u_{mig}}$$

$$= \frac{\tau}{Pe} \left| \frac{\pm \frac{1}{2} - y'_{e\pm}}{y'_{e\pm} + 8y'_{e\pm}/(1 - 4y'_{e\pm}{}^2)} \right|, \quad (12)$$

where u_{mig} is evaluated at $y'_{e\pm}$. τ/Pe is an alternative time constant for this problem, as noted by King and Leighton.⁹ When $Pe=30$, $\tau_e=0.005 \tau$, so that the transient profile shown in Fig. 3 is at approximately $0.2 \tau_e$. As expected, at these short times, the width of the denuded zone is considerably less than the final steady state.

Transient behavior can also be induced by drop coalescence. If coalescence is slow compared to τ , however, quasi-steady-state concentration profiles result.

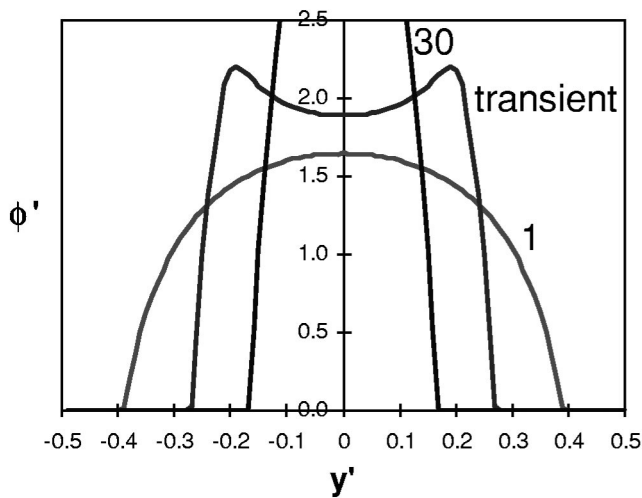


FIG. 3. A temporal solution after sudden increase in Pe from 1 to 30, and $\beta=0$. Shown are solutions for the initial and final single-mode steady states, and the transient bimodal distribution at $t'=0.001$.

III. MATERIALS AND EXPERIMENTAL METHODS

Three fluids were used in this study: poly(ethylene glycol) (PEG, the continuous phase; PolySciences²⁰), poly(propylene glycol) (PPG; Arco Chemical Co.) and poly(ethylene-alt-propylene) (PEP, Polymer Synthesis Facility, U. Minnesota). Their number-average molecular masses are 10 000, 12 200 and 4300, respectively; the polydispersity of molecular mass for each is approximately $M_w/M_n=1.1$, as determined by matrix-assisted laser-desorption-ionization mass spectroscopy and size-exclusion chromatography.

Experiments were conducted at 75 and 90 ± 0.1 °C. Viscosities were measured using Carrimed and ARES cone-and-plate rheometers (Table I) and found to be Newtonian up to shear rates of at least 800 s^{-1} . Since the viscosity of PPG and PEP are similar, the viscosity ratio $\hat{\eta}$ is essentially constant and equal to 0.18. Densities ρ were computed (Table I) based on tabulated reference data according to the following:²¹

$$1/\rho = 1/\rho_{\text{ref}} + e(T - T_{\text{ref}}), \quad (13)$$

where ρ_{ref} is the density at T_{ref} .

The interfacial tension between drop and continuous phases was determined from measurement of small deformation under steady shear^{22,23} and by the droplet retraction technique.²⁴ The interfacial tension of PPG/PEG is 0.0034 and 0.0030 N/m at 75 and 90 °C, respectively.²⁵ The interfacial tension of PEP/PEG is 0.010 N/m at 90 °C, cf. Refs. 26, 27.

TABLE I. Material viscosity and density.

Material	T (°C)	η (Pa s)	ρ (g/cm ³)
PEG 10 k	75	4.1	1.081
	90	2.7	1.070
PPG 12.2 k	75	0.71	0.970
	90	0.50	0.960
PEP 4.3 k	75	0.91	0.826
	90	0.48	0.817

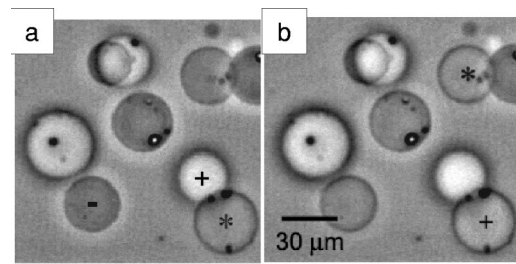


FIG. 4. Two images from a through-focus series of images of the same area of the sample. The previous shear rate was 5 s^{-1} , $h=200 \mu\text{m}$, and $a_v = 17 \mu\text{m}$. The focal plane is at (a) $y=35$ and (b) $y=50 \mu\text{m}$. The variation in the appearance of the drops indicates their position relative to the plane of focus. Dark (under-focused) drops (e.g., labeled with a minus sign) are closer to the objective lens, and white (over-focused) drops (e.g., labeled with a plus sign) are further away. Drops near the plane of focus (labeled with an asterisk) exhibit weaker contrast, such that the interior of the drop has nearly the same intensity as the surroundings and only its rim appears dark. Note that a light “halo” surrounds under-focused drops, whereas over-focused drops are surrounded by a dark one.

Mixtures were examined by bright-field optical microscopy using a Linkam Scientific Instruments CSS-450 heated shearing cell that was mounted on a Zeiss microscope equipped with a 640×480 pixel CCD camera. One of two $10 \times$ long-working-distance objectives was used, and the image magnification (0.81 and $0.66 \mu\text{m}/\text{pixel}$, respectively) was determined using a calibrated Ronchi ruling. The shear cell has a parallel-plate geometry;²⁵ the gap spacing was calibrated by means of the microscope stage micrometer by focusing on the top and bottom plate surfaces. The translation of the micrometer is linear and accurate to within 0.8%, tested independently using a dial gauge micrometer. The experimental uncertainty of the gap spacing is approximately $\pm 4 \mu\text{m}$.

Mixtures were prepared by weighting the components, and stirring them with a spatula. After loading the mixture into the shear stage, the gap was set as desired. If another gap spacing was desired, the sample was stirred again and reloaded, before setting the gap, so that initial conditions would be consistent. The sample was sheared at a desired rate for times $O(1000 \text{ s})$, or longer, in intervals of approximately 100 s. After such long shearing times, the drop-size distribution was relatively narrow, with $a_v/a_n \approx 1.2$. (a_v and a_n denote volume and number averaged radii, respectively, and were computed according to procedures described earlier.²⁸) Immediately after shearing, when the sample was at rest, a series of images were obtained at different planes of focus (Fig. 4). The distance between successive planes of focus is approximately equal to the translation of the microscope stage micrometer times the refractive index of PEG $n_{\text{PEG}}=1.46$.²⁹ Rest times were limited $O(100 \text{ s})$, so that buoyant motion during rest could be neglected. [For example, PEP drops, $a=10 \mu\text{m}$, in PEG at 90 °C rise at a rate equal to 27 nm/s —Eq. (4).] The drop concentration, gap setting, and shear rate were selected to facilitate measurement of the drop concentration profile: viz., so that images of drops would not overlap significantly and so that $a/h < 10$. Owing partly to these requirements, the range of Pe tested was limited. [Note that for all experiments, the Reynolds

TABLE II. Summary of experimental conditions and data analysis.^a

Drop matl	PEP	PEP	PPG	PPG
ϕ_0	0.0200	0.0200	0.0220	0.0220
T (°C)	90	90	75	90
$\hat{\eta}$	0.18	0.18	0.17	0.19
h (μm)	200	200	150	100
$\dot{\gamma}$ (s^{-1})	5	20	40	80
a_v (μm)	17	10	8.5	6.0
Ca	0.02	0.05	0.40	0.40
β	2.7	0.46	0.006	0.003
N_f	13	28	15	8
N_d	352	1329	362	244
f_y	0.038	0.042	0.050	0.050
Pe	1.0 ± 0.2	2.0 ± 0.5	11.0 ± 1.4	10.1 ± 0.7
$\langle \Delta^2 \rangle^{1/2} / \sqrt{N_f}$	0.02	0.02	0.02	0.02
f_{gy}	0.21	0.16	0.22	0.25
f_{gy}/f_y	5.5	3.7	4.4	5.0

^aThe standard uncertainty in h and a_v are ± 4 and ± 1 μm , respectively, based on one standard deviation. N_f is the total number of images in the focal series, and N_d is the total number of drops counted. Here f_y is estimated by interpolation of the calculations of Loewenberg and Hinch, as a function of $\hat{\eta}$ and Ca (Ref. 15).

number $\text{Re} = \rho_c \dot{\gamma} h^2 / \eta_c$ is small ($\approx 10^{-6}$), so that Stokes flow can be assumed.]

For each series of images, the number of drops in focus in each image was recorded (e.g., see Fig. 4). The number density was normalized to give unit integral across the gap, so that it could be fit directly with the normalized concentration [Eq. (10)] by adjusting Pe. From Pe, the drop gradient diffusivity f_{gy} was determined.

IV. RESULTS AND DISCUSSION

Experimental conditions and results are summarized in Table II, and an example data set is shown in Fig. 5. Wide

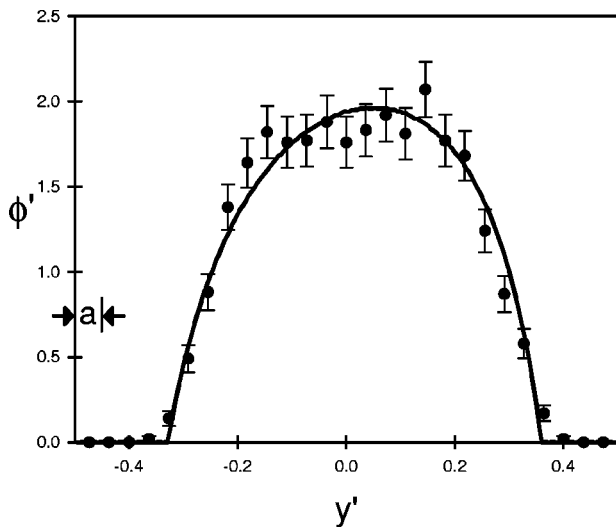


FIG. 5. Theoretical and experimental volume fraction profiles are compared. Symbols represent data from PEP drops ($\phi = 0.0200$) sheared at 20 s^{-1} ; see Table II for detailed parameters and results, error bars represent standard uncertainties. The solid curve is the best-fit line from Eq. (10), where $\text{Pe} = 2.0$. The volume-averaged drop radius ($a_v = 10 \mu\text{m}$) is indicated at left. The gap spacing is $200 \mu\text{m}$.

denuded zones adjacent to each wall are evident (Fig. 5). These denuded zones are clearly not an excluded volume effect, because they each are much wider than the drop radius. The experimental concentration profile is fit to the theoretical profile [Eq. (10)], by adjusting the value of Pe to minimize the sum of squared errors ($\Sigma \Delta^2$). The uncertainty in Pe is estimated from the values of Pe that cause this error sum to double. From the value of Pe, we deduce the only unknown material parameter, i.e., f_{gy} (Table II). Since an estimate of f_y (Table II) is available by interpolation of published results,¹⁵ we calculate the unknown parameter f_{gy}/f_y . The uncertainty in this ratio is essentially the same in proportion as the uncertainty in Pe. The ratio f_{gy}/f_y does not depend significantly on Ca (for Ca ranging from 0.02 to 0.4). Averaging the four experiments, $f_{gy}/f_y = 4.6 \pm 0.8$. This value is somewhat smaller than the value 6 that was calculated for rigid rough spheres.¹⁸ Although no calculations are published, f_{gy}/f_y is expected to be roughly of this magnitude also for fluid drops.⁹

These results differ from those previously reported by King and Leighton,⁹ who found values of f_{gy} equal to roughly 0.02, approximately an order of magnitude smaller than our current measurements. King and Leighton suggested three possible reasons to explain their unexpectedly small values. Of these, the most significant difference with the present experiments and likely the most significant effect is partial immobilization of the interface induced by the presence of surfactant. (Concerning the other two suggestions, coalescence is rare and size polydispersity is only a minor effect.⁹) The diffusivity of drops with completely immobile interfaces is expected to be indeed very small.³⁰

Although the interfaces (in the experiments of King and Leighton) were, by design, far from being completely immobile,^{9,31} the effectiveness of the surfactant in inhibiting coalescence is consistent with a partial reduction in the interfacial mobility. Such reduction can influence the coalescence process in one or two ways. First, as the mobility of the interface decreases, either by increasing drop viscosity or adding surfactant, the trajectory of colliding drops approaches that exhibited by solid particles.³² Second, at large enough Ca, lower interface mobility *also* suppresses film drainage, and thereby further inhibits coalescence. In relation to shear-induced drop diffusion, the effect of surfactant on the drop trajectory is the central issue.

In the present experiments, the interfaces are clean, without surfactant. Surfactant is not necessary to prevent coalescence, because both phases are somewhat more viscous than the fluids used by King and Leighton. Consequently, the coalescence rate is small. In addition, the experiments involving PPG drops are essentially at Ca_{crit} , where the coalescence rate is negligible.

We now estimate the approximate degree of interface immobilization in the experiments of King and Leighton and the magnitude of its effect on the diffusivity. The gradient in the interfacial surfactant concentration caused by drop convection may be limited by any of three factors:^{33,34} diffusion (of surfactant) on the interface, diffusion in the bulk (to and from the interface), and local equilibration between the interface and the adjacent regions. Specifically, the concentration

gradient is associated with at least one of three parameters, depending the dominant (limiting) mechanism: Pe_σ (the interfacial Peclet number), $Pe_b \cdot H$ (the product of the bulk Peclet number and the dimensionless diffusion distance), $\dot{\gamma}/k$ (the ratio of the shear rate to the kinetic rate constant for desorption, i.e., the inverse of the Biot number), respectively. Of the three, only $Pe_b \cdot H$ depends significantly on surfactant concentration. The interfacial gradient induces a Marangoni stress that retards the interface, which is proportional to the product of Ma (the Marangoni number) and the appropriate parameter associated with the concentration gradient.^{32,35}

The Marangoni stress depends on surfactant volume fraction ϕ_s in such a way that at very low concentration, it increases with ϕ_s and then it *decreases* again at high concentrations, when surfactant exchange with the bulk is dominant. In the latter “remobilization” regime,^{31,36} increasing surfactant concentration mainly reduces the diffusion distance H .

For King and Leighton’s experiments ($\dot{\gamma} \approx 10 \text{ s}^{-1}$; $a \approx 300 \text{ } \mu\text{m}$), we estimate $Pe_\sigma \approx Pe_b = \dot{\gamma} a^2 / D_s \approx 3 \times 10^3$ and

$$H \approx \frac{\Gamma_{\max} v_s}{(\phi_s + \phi_{sc}) a} \approx 5 \times 10^{-3},$$

so that bulk diffusion is far more effective than surface diffusion in reducing interfacial concentration gradients. In other words, the interface is remobilized to a significant extent. (These estimates involve the following parameters: the surfactant diffusion coefficient $D_s \approx 2.6 \times 10^{-10} \text{ m}^2/\text{s}$;^{31,37} the molecular volume of the surfactant $v_s \approx 1 \text{ nm}^3$; the maximum interfacial concentration $\Gamma_{\max} \approx 1 \text{ nm}^{-2}$;³⁷ and the volume fraction of surfactant in the aqueous phase $\phi_s \approx 0.0009$, which is approximately 1500 times greater than the characteristic concentration ϕ_{sc} .^{31,37}) To obtain the largest estimate of remobilization, we also assume that the interfacial kinetics are fast enough (i.e., $k > 1 \text{ s}^{-1}$, approximately an order of magnitude larger than the *lower bound* estimate suggested by Stebe *et al.*³¹) that surfactant exchange with the bulk is limited by diffusion. Considering drop viscosity and Marangoni effects together,³⁸ the interfacial mobility is proportional to approximately $1/(3 + 3 \hat{\eta} + Ma Pe_b H)$. Ma can be estimated as

$$Ma \approx \frac{\sigma_0 - \sigma}{\sigma_0 Ca},$$

where σ_0 is the interfacial tension in the absence of surfactant, $(\sigma_0 - \sigma)$ is the surface pressure, and Ca is the capillary number. In King and Leighton’s experiments, Ma is near unity. In view of an approximately analogous relationship between $\hat{\eta}$ and $Ma Pe_b H$, we conclude that $Ma Pe_b H$ is large enough [$O(10)$] that a significant effect on the drop diffusivity is possible,¹⁵ in spite of rapid exchange of surfactant with the bulk. Note that reducing the interface mobility by means of Marangoni effects will have a much greater effect on diffusivity than on wall migration, because of differences in local flow type: the former involves drop interaction (local interface extension), whereas the latter is associated with single drop behavior (interface recirculation).

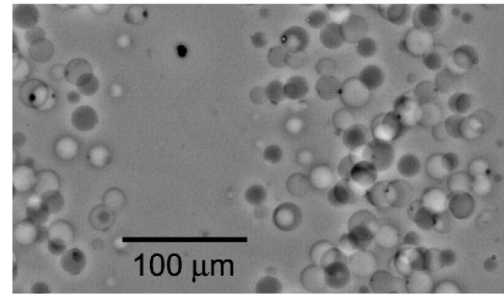


FIG. 6. Trains of drops that develop after extended shearing times when drop size and Ca are large enough. The image is taken at rest after shearing at 100 s^{-1} for 200 s. The volume average drop radius is $a_v = 9.1 \text{ } \mu\text{m}$, so that $Ca = 0.25$. The gap spacing h is $200 \text{ } \mu\text{m}$. Essentially the full width of the band on the right is in view. As in Fig. 4, drops have various light and dark appearance.

While the focus of this report is migration along the velocity gradient direction (y), we close this section by reporting interesting observations of migration along the vorticity axis (z). Global migration along the vorticity axis is predicted to be negligible,³⁹ and indeed none is observed. However, bands of high and low drop concentration (Fig. 6) develop under some conditions, most readily when drop size and Ca are relatively large (see caption, Fig. 6). Bands were observed in mixtures containing either PPG or PEP drops. Demonstrating the importance of large drop size, these stripes may be erased by shearing at high rates, so that the drops break to a much smaller size and eventually redistribute by shear-induced diffusion along z . Demonstrating the importance of large Ca , weak stripes (those that have just begun to form, so that the concentration of drops is only slightly nonuniform) can also be erased by shearing at slower rates, though the rate of erasure is much slower. Such erasure may be prevented, if the rate of coalescence is fast enough. (When coalescence is dominant, string and “pearl-necklace” morphologies have been observed.^{1,40}) It was not possible to obtain uniform (along z) mixtures with sufficiently large PEP drops at high Ca (Table II). Consequently, analysis of $\phi(y)$ for this material was restricted to lower values of Ca . In all experiments analyzed according to Eq. (10), the concentration of drops along the vorticity axis was uniform.

A nonuniform organization of dispersed phase along the vorticity axis is also found in coating flows of suspensions of rigid particles.⁴¹ The coating flow field was realized in a Couette device partially filled with the suspension.⁴¹ When the device was completely filled, no such segregation of particles was observed. These and related phenomena have been discussed theoretically, e.g., Refs. 42 and 43, and additional theoretical work is needed.

V. IMPLICATIONS

This work demonstrates that wall migration in fluid suspensions may be significant, with important implications. First, this phenomenon has significant effects on coalescence behavior, because the concentration of disperse phase is higher in the center of the gap, thereby increasing the coalescence rate.²⁵ To approximate the magnitude of this effect,

we recall that coalescence of moderately dilute suspensions involves collisions between pairs of droplets, and that the collision frequency per unit volume is proportional to ϕ^2 . Therefore, the effective concentration for coalescence is not ϕ_0 . Rather, to leading order it is²⁵

$$\phi_{\text{eff}} = \frac{\langle \phi^2 \rangle}{\phi_0}. \quad (14)$$

Wall migration and drop banding phenomena also contribute in other ways to morphology development. For example, when the average volume fraction is high enough, the mid-plane volume fraction becomes large enough that continuous thread formation is possible.^{1,40} Wall migration has a crucial practical influence on the surface appearance and surface properties of extruded and molded parts.

VI. CONCLUSIONS

The steady-state profile of the volume fraction of dispersed phase produced by the balance of wall migration and shear-induced diffusion is calculated for simple shear, without any linearization approximation for the drop migration velocity, valid for all values of Pe [Eq. (10)], thereby extending an earlier analysis⁹ that is valid in the limit of high Pe (>10). The effect of buoyancy is also described. This analysis was used to obtain the first experimental measurements of drop diffusivity in emulsions with clean interfaces. These results differ significantly from previous results from an emulsion containing surfactant, and the effect of surfactant on drop diffusivity is discussed. The experimental gradient diffusivity is approximately 4 to 5 times larger than published predictions of the self-diffusivity. Under conditions of sufficiently large Ca and drop size, migration in the vorticity direction was also observed.

ACKNOWLEDGMENTS

Partial financial support by NSF Grant No. CTS-9731502 is acknowledged gratefully. The author thanks Professor J. F. Brady and Dr. A. Zinchenko for discussions that prompted this study.

¹K. B. Migler, "String formation in sheared polymer blends: Coalescence, breakup, and finite size effects," *Phys. Rev. Lett.* **86**, 1023 (2001).

²A. Karnis and S. G. Mason, "Particle motions in sheared suspensions XXIII. Wall migration of fluid drops," *J. Colloid Interface Sci.* **24**, 164 (1967).

³C. E. Chaffey, H. Brenner, and S. G. Mason, "Particle motions in sheared suspensions XVIII. Wall migration (theoretical)," *Rheol. Acta* **4**, 64 (1965).

⁴C. E. Chaffey, H. Brenner, and S. G. Mason, "Correction. Particle motions in sheared suspensions XVIII. Wall migration (theoretical)," *Rheol. Acta* **6**, 100 (1967).

⁵P. C. H. Chan and L. G. Leal, "Motion of a deformable drop in a 2nd-order fluid," *J. Fluid Mech.* **92**, 131 (1979).

⁶J. R. Smart and D. T. Leighton, "Measurement of the drift of a droplet due to the presence of a plane," *Phys. Fluids A* **3**, 21 (1991).

⁷T. Imaeda, "Sheer-induced migration of a droplet in the presence of a plane wall," *Physica A* **285**, 306 (2000).

⁸P. C. H. Chan and L. G. Leal, "An experimental-study of drop migration in shear-flow between concentric cylinders," *Int. J. Multiphase Flow* **7**, 83 (1981).

⁹M. R. King and D. T. Leighton, "Measurement of shear-induced dispersion in a dilute emulsion," *Phys. Fluids* **13**, 397 (2001).

¹⁰W. S. J. Uijttewaai, E. J. Nijhof, and R. M. Heethaar, "Droplet migration, deformation, and orientation in the presence of a plane wall—A numerical study compared with analytical theories," *Phys. Fluids A* **5**, 819 (1993).

¹¹W. S. J. Uijttewaai and E. J. Nijhof, "The motion of a droplet subjected to linear shear-flow including the presence of a plane wall," *J. Fluid Mech.* **302**, 45 (1995).

¹²M. R. Kennedy, C. Pozrikidis, and R. Skalak, "Motion and deformation of liquid-drops, and the rheology of dilute emulsions in simple shear-flow," *Comput. Fluids* **23**, 251 (1994).

¹³J. Hadamard, "Mouvement permanent lent d'une sphere liquide et visqueuse dans un liquide visqueux," *C. R. Hebd. Seances Acad. Sci.* **152**, 1735 (1911).

¹⁴R. S. Allan and S. G. Mason, "Particle motions in sheared suspensions XIV. Coalescence of liquid drops in electric and shear fields," *J. Colloid Interface Sci.* **17**, 383 (1962).

¹⁵M. Loewenberg and E. J. Hinch, "Collision of two deformable drops in shear flow," *J. Fluid Mech.* **338**, 299 (1997).

¹⁶S. Guido and M. Simeone, "Binary collision of drops in simple shear flow by computer-assisted video optical microscopy," *J. Fluid Mech.* **357**, 1 (1998).

¹⁷X. F. Li and C. Pozrikidis, "Wall-bounded shear flow and channel flow of suspensions of liquid drops," *Int. J. Multiphase Flow* **26**, 1247 (2000).

¹⁸F. R. daCunha and E. J. Hinch, "Shear-induced dispersion in a dilute suspension of rough spheres," *J. Fluid Mech.* **309**, 211 (1996).

¹⁹T. Hashimoto, K. Matsuzaka, and K. Fujioka, "Formation of droplets with a very narrow size distribution in mixtures subjected to shear flow. I. Shear rate dependence," *J. Chem. Phys.* **108**, 6963 (1998).

²⁰Certain commercial materials and equipment are identified in this paper in order to adequately specify the experimental procedure. In no case does such identification imply recommendation or endorsement by the National Institute of Standards and Technology, nor does it imply that these are necessarily the best available for the purpose.

²¹D. W. VanKrevelen, *Properties of Polymers. Their Correlation with Chemical Structure; Their Numerical Estimation and Prediction from Group Contributions*, 3rd ed. (Elsevier, Amsterdam, 1990).

²²G. I. Taylor, "The viscosity of a fluid containing small drops of another fluid," *Proc. R. Soc. London, Ser. A* **138**, 41 (1932).

²³J. M. Rallison, "The deformation of small viscous drops and bubbles in shear flows," *Annu. Rev. Fluid Mech.* **16**, 45 (1984).

²⁴A. Luciani, M. F. Champagne, and L. A. Utracki, "Interfacial tension coefficient from the retraction of ellipsoidal drops," *J. Polym. Sci., Part B: Polym. Phys.* **35**, 1393 (1997).

²⁵B. E. Burkhart, P. V. Gopalkrishnan, S. D. Hudson, A. M. Jamieson, M. A. Rother, and R. H. Davis, "Droplet growth by coalescence in binary fluid mixtures," *Phys. Rev. Lett.* **87**, 098304 (2001).

²⁶R.-J. Roe, "Interfacial tension between polymer liquids," *J. Colloid Interface Sci.* **31**, 228 (1969).

²⁷U. Jorzik and B. A. Wolf, "Reduction of the interfacial tension between poly(dimethylsiloxane) and poly(ethylene oxide) by block copolymers: Effects of molecular architecture and chemical composition," *Macromolecules* **30**, 4713 (1997).

²⁸A. J. Ramic, S. D. Hudson, A. M. Jamieson, and I. Manas-Zloczower, "Temporary droplet-size hysteresis in immiscible polymer blends," *Polymer* **41**, 6263 (2000).

²⁹J. Brandrup, E. H. Immergut, and E. A. Grulke, *Polymer Handbook* (Wiley, New York, 1999).

³⁰G. K. Batchelor and J. T. Green, "The hydrodynamic interaction of two small freely-moving spheres in a linear flow field," *J. Fluid Mech.* **56**, 375 (1972).

³¹K. J. Stebe, S. Y. Lin, and C. Maldarelli, "Remobilizing surfactant retarded fluid particle interfaces. 1. Stress-free conditions at the interfaces of micellar solutions of surfactants with fast sorption kinetics," *Phys. Fluids A* **3**, 3 (1991).

³²J. Blawdziewicz, E. Wajnryb, and M. Loewenberg, "Hydrodynamic interactions and collision efficiencies of spherical drops covered with an incompressible surfactant film," *J. Fluid Mech.* **395**, 29 (1999).

³³J. A. Holbrook and M. D. Levan, "Retardation of droplet motion by surfactant. 2. Numerical-solutions for exterior diffusion, surface-diffusion, and adsorption-kinetics," *Chem. Eng. Commun.* **20**, 273 (1983).

³⁴J. A. Holbrook and M. D. Levan, "Retardation of droplet motion by surfactant. 1. Theoretical development and asymptotic solutions," *Chem. Eng. Commun.* **20**, 191 (1983).

- ³⁵Y. P. Wang, D. T. Papageorgiou, and C. Maldarelli, "Increased mobility of a surfactant-retarded bubble at high bulk concentrations," *J. Fluid Mech.* **390**, 251 (1999).
- ³⁶K. J. Stebe and C. Maldarelli, "Remobilizing surfactant retarded fluid particle interfaces. 2. Controlling the surface mobility at interfaces of solutions containing surface-active components," *J. Colloid Interface Sci.* **163**, 177 (1994).
- ³⁷S. Y. Lin, K. McKeigue, and C. Maldarelli, "Diffusion-controlled surfactant adsorption studied by pendant drop digitization," *AIChE J.* **36**, 1785 (1990).
- ³⁸J. A. Ramirez and R. H. Davis, "Mass transfer to a surfactant-covered bubble or drop," *AIChE J.* **45**, 1355 (1999).
- ³⁹H. L. Goldsmith and S. G. Mason, "The microrheology of dispersions," Chapter 2 in *Rheology: Theory and Applications*, edited by F. R. Eirich (Academic, New York, 1967), Vol. 4, pp. 85–250.
- ⁴⁰J. A. Pathak, M. C. Davis, S. D. Hudson, and K. B. Migler, "Layered droplet microstructures in sheared emulsions: Finite-size effects," *J. Colloid Interface Sci.* **255**, 391 (2002).
- ⁴¹M. Tirumkudulu, A. Mileo, and A. Acrivos, "Particle segregation in monodisperse sheared suspensions in a partially filled rotating horizontal cylinder," *Phys. Fluids* **12**, 1615 (2000).
- ⁴²R. Mauri and D. T. Papageorgiou, "The onset of particle segregation in plane Couette flows of concentrated suspensions," *Int. J. Multiphase Flow* **28**, 127 (2002).
- ⁴³J. F. Brady and I. C. Carpen, "Second normal stress jump instability in non-Newtonian fluids," *J. Non-Newtonian Fluid Mech.* **102**, 219 (2002).